PCCP

Accepted Manuscript

ROYAL SOCIETY OF CHEMISTRY

www.rsc.org/pccp

PCCP

ARTICLE

Inclusion of supported gold nanoparticles into their semiconductor support

Marcus Lau, Anna Ziefuss, Tim Komossa and Stephan Barcikowski

Received 00th January 20xx,
Accepted 00th January 20xx

DOI: 10.1039/x0xx00000x

www.rsc.org/

Supported particles are easily accessible as standard materials used in heterogeneous catalysis and photocatalysis. This article addresses our exemplary studies on the integration of supported nanoparticles into their solid support, namely gold nanoparticles into zinc oxide sub-micrometer spheres by controlled pulsed laser melting in a free liquid jet. This one-step, continuous flow-through processing route reverses the educt´s structure, converting the ligand-free surface adsorbate into a spherical subsurface solid inclusion within its former support. The results show how a nanoparticulate surface adsorbate can be included in form of crystalline nanoparticles into the resolidified support matrix demonstrated by using plasmonic nanoparticles and semiconductor microparticles as reference materials.

Introduction

Supported metal nanoparticles on metal oxides are commonly available raw materials with application prospects in catalysis [1-3]. For example, gold nanoparticles (Au NP) on zinc oxide (ZnO) support catalyze chemical reactions [4]. Even though gold nanoparticles (Au NP) can be easily attached to ZnO nanoparticles [5, 6] the integration into zinc oxides matrix on the nanoscale is challenging. A possibility to melt aqueous dispersions of particulate materials under non-equilibrium conditions is the pulsed laser melting in liquid (PLML). PLML has been shown to be an effective synthesis route for crystalline sub-micrometer spheres (SMS), but additive PLML has only rarely been investigated and did not cover supported particles yet.

Fabrication of SMS by PLML is a technique pioneered by Koshizaki and coworkers [7, 8]. Early application examples have been demonstrated by Hu et al. for SMS in lubricant oils to reduce the friction coefficient [9] and Fujiwara et al. used ZnO SMS as light emitting laser source [10].

Since the first report several articles report the possibility and power of this technique. In contrast to size-reducing pulsed laser fragmentation (PLFL), lower laser fluences are required, resulting in particle melting and resolidification as spheres. Wang et al. found onset laser fluence for particle melting of zinc oxide to be between 33 mJ/cm² and 67 mJ/cm² [8]. A limitation to high laser fluences was reported by Wang et al. for the laser melting of CuO nanoparticles to copper SMS [11]. At a fluence of 150 mJ/cm² the SMS showed a rough surface. This indicates a less effective particle melting due to onset of particle fragmentation. The influence of educt particle size on melting effectivity was demonstrated by Tsuji et al. [12]. They showed that by increasing the educt particle size of ZnO particles the fluence required for sufficient PLML to receive monomodal and smooth ZnO SMS increases. Namely 70 nm ZnO educt particles were molten completely at fluences of 100 mJ/cm² whereas aggregated (500 nm aggregate diameter) ZnO educt particles were only partially molten at laser fluences of 200 mJ/cm² and completely at fluences of 300 mJ/cm² [12]. Liu et al. demonstrated that PLML appears as isochoric process using octaedrical Au NP and transformed them into monodisperse Au nanospheres preserving the volume of the particles, thus demonstrating that PLML can be applied as isochoric particle reshaping [13].

First reports on laser melting of Au NP were given by El-Sayed and coworkers [14-16] who reported the sufficient interaction of surface plasmons with 532 nm laser light by isochoric melting of Au nanorods to nanospheres. In 2005 Inasawa et al. showed that for gold nanoparticles the melting temperature is approximately 100 K below the value of the bulk material using nanoparticles around 38 nm and applying a laser wavelength on 355 nm [17]. Tsuji and coworkers recently reported the possibilities to melt aggregated Au NP to SMS with 532 nm laser light and found a PLML induction time interval caused by the laser-induced surfactant removal [18, 19].

Studies on SMS formation mostly report 355 nm laser wavelength and nanosecond pulses to cause distinctive particle melting in liquid, even though other wavelengths and pulse lengths are able to cause (partial) melting as well [20].

Besides simple physical melting also changes in chemical composition are reported [7, 11, 21]. Ishikawa et al. studied the formation of boron carbide SMS particles from boron nanoparticles in organic solvents. Additionally, PLML-alloying of non-equilibrium phases is known [22]. Swiatkowska-Warkocka et

Technical Chemistry I, University of Duisburg-Essen and Center for Nanointegration Duisburg-Essen (CENIDE), Universitaetsstr. 7, 45141 Essen, Germany.

Electronic Supplementary Information (ESI) available showing further characterization of the material before and after laser melting. The characterization includes determination of particle load on support from different approaches, optical characterization, particle size distributions and additional SEM images. See DOI: 10.1039/x0xx00000x

al. generated bimetallic crystalline SMS of copper and gold. But they obtained a solid solution in contrast to an inclusion type SMS reported here. Nakamura et al. recently reported on magnetite particles integrated into calcium phosphate SMS by combination of chemical precipitation and laser wavelength absorbant by the iron salt, subsequently integrated into the calcium salt SMS during PLML [23]. Hence, investigation on integration of iron into SMS include chemical reaction and complex precipitation-reaction-melting interdependence [23]. Next to reactive PLML or alloying of miscible elements the question arises what happens during the irradiation of partly miscible or immiscible mixtures under PLML conditions. PLML a colloidal mixture of gold with as-prepared iron oxide nanoparticles resulted in core-shell structure with porous surface after Fe etching [24-26]. But supported particles are not yet investigated.

In this context the facile synthesis of supported particles comes into play, such as adsorption of ligand-free metal nanoparticles (Au, Ag, Pt, Pd) on supports (ZnO, TiO2, BaSO4, Graphene) [27] simply by mixing at defined liquid parameters [28] thus achieving up to 60 wt% NP-on-support at 100% yield. Taking Au/ZnO as relevant example (e.g. for photocatalysis applications), it is open what happens if this nano/micro support system is exposed to PLML.

Experimental

Preparation of supported particles follows mechanism firstly reported by Wagener et al.[27] and described in detail by Marzun et al. [28], where Au/ZnO preparation procedure was analogous to Lau et al. [6]. Au NP were generated by picosecond pulsed laser ablation in liquids (PLAL) in 600 µM aqueous phosphate buffer to receive small particles and size separation was conducted by centrifugation using an Ultracentrifuge (Beckman Coulter), with a force of 30,000 g for 14 minutes resulting in a monodisperse Au NP colloid with defined concentration (see Fig. 1). Concentration of supernatant was determined from extinction at a fixed wavelength subsequent to calibration with different concentration of same particle size. The monodisperse Au colloid had a concentration of 62.7±0.1 µg/mL after centrifugation. We added 95 mg zinc oxide particles to an overall colloid volume of 450 mL Au NP in water resulting in an Au NP loading of 30 wt% referred to zinc oxide after 100 % Au NP adsorption. Detailed particle size distributions (mass-weighted 5±0.9 nm, number weighted 4.7±0.8 nm) and determination of concentration by calibrated UV-vis spectroscopy of the monodisperse Au NP colloids (polydispersity index < 0.03) are provided in Fig. S1 of supporting information. Zinc oxide particles (Sigma Aldrich) were simply added to the monodisperse gold nanoparticle suspensions and the obtained gold/zinc oxide supported particle powder was dried (50°C, 8h). Note that there are different values describing the amount of supported nanoparticles. Fig. S2 illustrates the absolute wt% of nanoparticles plotted versus the wt% of gold nanoparticles referred to zinc oxide as support, resulting in nonlinear correlation between the wt% and vol%. The volume percentage might be of interest as optical response and colloidal analytics often correlate to the particle volume. But in catalysis application wt% is the standard unit. For PLML the highest amount of supported gold nanoparticles used in this study was 30 wt% of gold referred to the support (thus a gold amount of approx. 23 wt% absolute), equivalent to 11 vol% (see Fig. S2).

Laser irradiation was performed with an Nd:YAG laser operating at the 3rd harmonic (355 nm wavelength) with 85 kHz repetition rate, 23 watts and a pulse length of 40 ns.

For determination of the influence of laser fluence on PLML and defined volume-specific laser energy dose we used the design of a sequential liquid flow. This design has been reported previously and allows to study the impact of the applied laser fluence while focusing into a thin liquid filament [20]. Hence, minimized beam path in liquid significantly reduces fluence variation along propagation, allowing defined energy balancing. As reported before, a strong shift of a local peak in the UV/vis spectrum can be attributed to sufficient PLML effect [20]. Thus, plotting the observed shift of this local peak can be used to draw conclusion for PLML efficiency and the applied laser fluence. To study the influence of the applied laser fluence pure zinc oxide particles were used. The determined optimized laser fluence was used for the further experiments of gold/zinc oxide hybrid particles.

PLML of the hybrids was conducted under optimized conditions found for pure zinc oxide in pure water with no additives. All used suspensions for laser irradiation had a particle concentration of 0.1 wt% as this was found to be appropriate to characterize PLFL and PLML sufficiently [20].

Size characterization of the particles was performed with an analytical disc centrifuge (CPS instruments) at 24,000 rpm, extinction of the colloids was determined with a UV-vis absorbance spectrometer (evolution 201) in a quartz glass cuvette. Diffuse powder reflection was determined in a spectrometer (Varian Cary) using a spectralon reference (PTFE). SEM images are taken with a SEM (FEI Quantana 400) on carbon supports. XRD measurements of the compound particles before and after PLML were carried out with a Cu K-α irradiation source at 40 kV and 40 mA in a Bruker D8 Advance system.

The preparation route for the nano/micro support systems used here is schematically shown in Fig. 1.

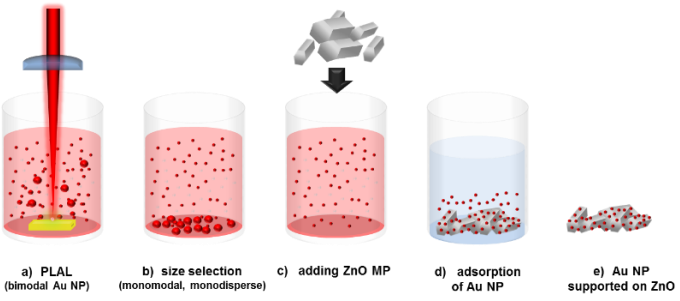

Fig. 1 Schematic illustration of the process steps to fabricate supported Au NP/ZnO MP with monodisperse nanoparticles attached to the support: a) picosecond-pulsed laser ablation in water (PLAL); b) size selection by centrifugation; c) addition of zinc oxide microparticles to the gold colloid; d) adsorption of gold nanoparticles onto the zinc oxide microparticles; e) dried powder for further PLML processing

Results and discussion

We demonstrate how plasmonic nanoparticles can be embedded into their semiconductor sub-micrometer spheres support by laser melting in continuous liquid flow. This route allows achieving an integration of metallic nanoparticles into a semiconductor SMS matrix in one step without performing any chemical synthesis. Within our experiments only pure water was used as carrier liquid. A fluid jet reactor setup was applied allowing precise fluence control and sequential analysis of the product evolution after defined PLML passage numbers. As shown in Fig. 2 a) variation of laser fluence results in significant shifts of the local UV-vis peak positions. Variation of laser fluence to determine the fluence regime for zinc oxide particle melting was performed with pure zinc oxide particles. Corresponding UV-vis spectra for pure zinc oxide from which peak shift is determined are shown in Fig. S3 in the supporting information. The bathochromic shift of the peak can be correlated to ZnO particle melting and resolidification as spheres. Thus plotting this shift versus the laser fluence illustrates the process window for PLML (at 355 nm laser wavelength and 40 ns pulse length) indicated in Fig. 2a) to be ≤ 0.2 J/cm². Fig. 2 b) shows powder scattering spectra for pure zinc oxide and for the supported Au NP on ZnO MP with 30 wt% gold loading. The diffuse reflection spectra show that increased extinction at wavelengths above 600 nm results from light scattering [29]. This diffuse reflection is caused from spheres formed by PLML proposed by Wang et al. [8]. That such spheres reflect light wavelengths in their size regime is confirmed here by scattering measurement of the dried particle powders. Additionally, absorption of Au NP Relative minimum in the scattering spectra around 550 nm) can be observed from diffuse reflection which becomes more distinctive after 50 passages PLML due to size increase of Au NP. UV-vis spectra before and after 50 passages of laser melting in liquid filament are shown in Fig. 2 c) and d) with SEM images of the corresponding educt and product particles as insert. For the semiconductor SMS products with gold nanoparticle inclusion two peaks in the visible regime are obtained. For the educt gold nanoparticle size a plasmon peak around 550 nm is observed. In the course of laser melting and reversing particle structure from supported Au NP to solid Au NP inclusions, obviously Au NP size increases as validated by SEM pictures (Fig. S5).

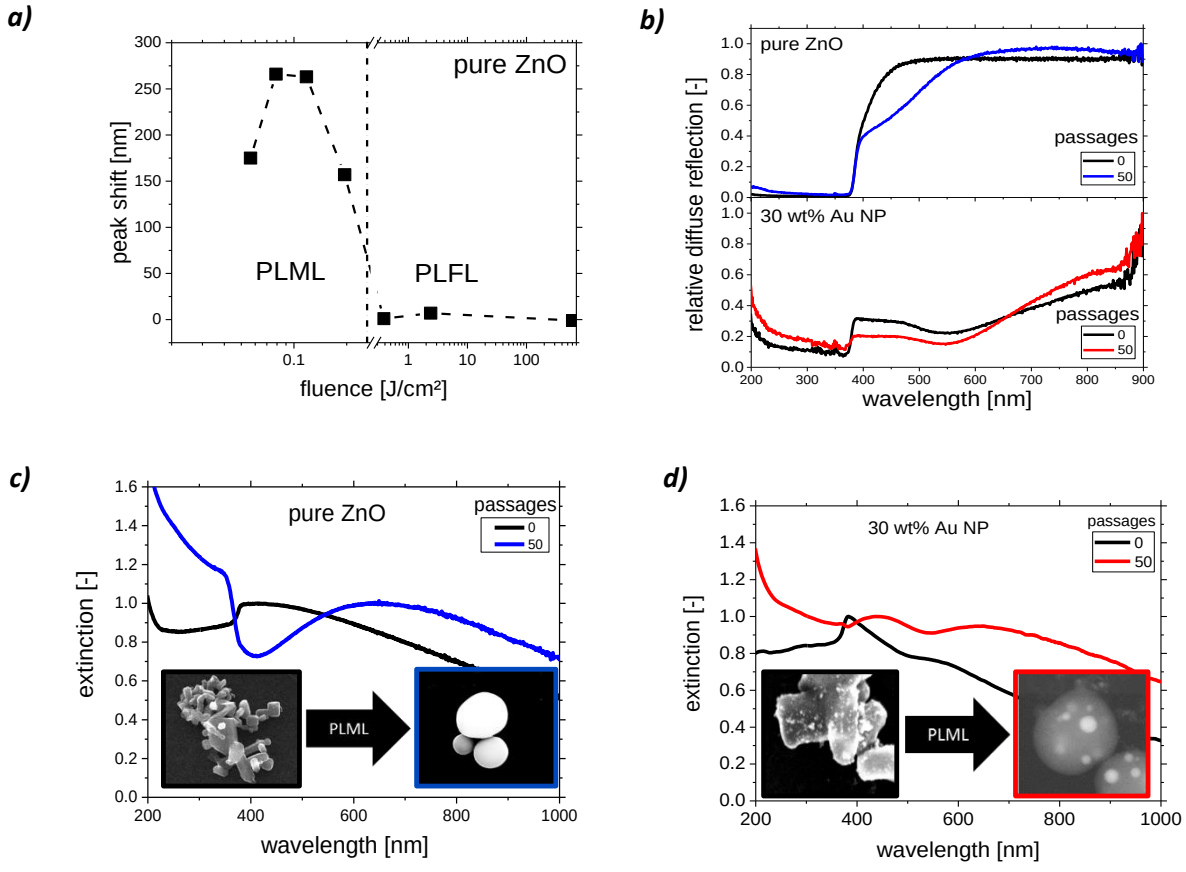

Fig. 2 a) impact of laser fluence on UV-vis peak shift of zinc oxide suspension after laser irradiation (at 355 nm and 40 ns); b) relative diffuse scattering of the dried particle powders before and after 50 passages PLML for pure ZnO (top) and 30 wt% Au NP supported on ZnO (bottom), respectively; c) normalized (at peak in visible regime) UV-vis spectrum of pure zinc oxide particles before (black line) and after (blue line) PLML in pure water; d) normalized UV-vis spectrum of zinc oxide particles with 30 wt% supported gold nanoparticles before (black line) and after (red line) PLML in pure water

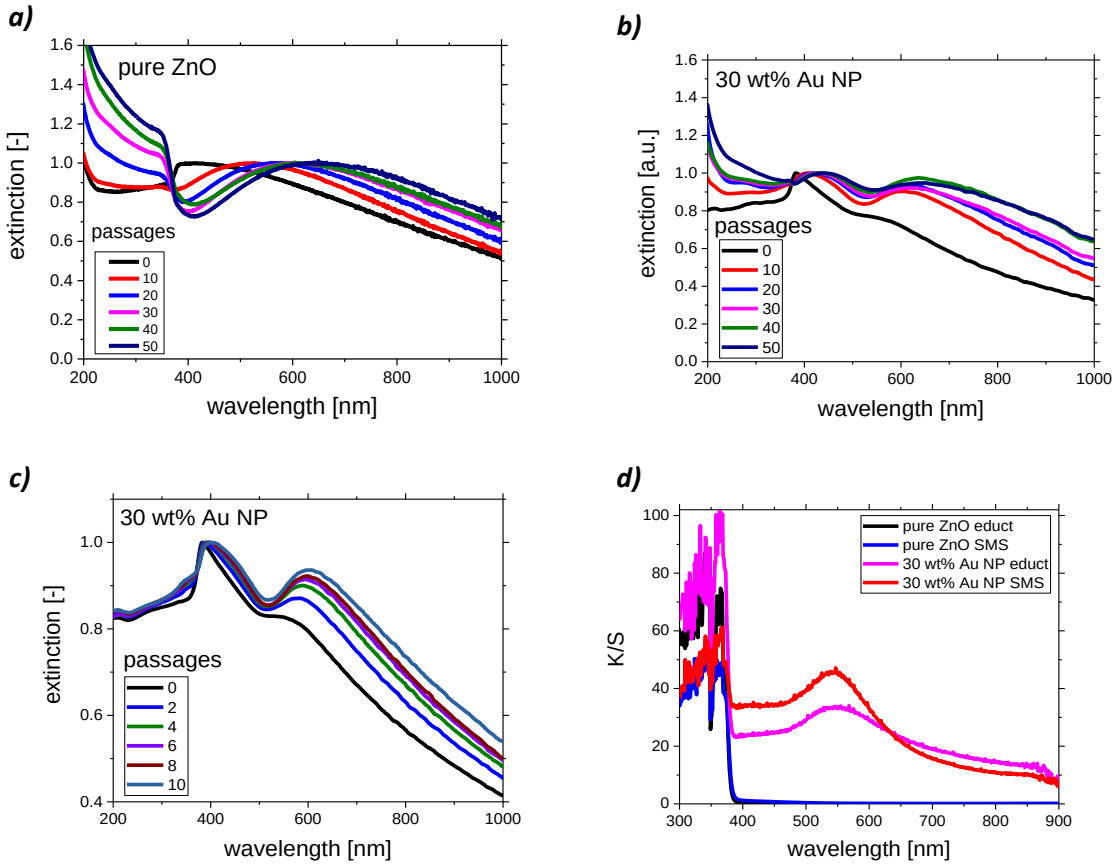

Fig. 3 Evolution of UV-vis spectra during PLML with a fluence of 80 mJ/cm² normalized at a peak in the visible regime for a) pure zinc oxide after each 10 passages from 0 to 50 irradiation cycles, for b) 30 wt% Au NP on ZnO after each 10 passages from 0 to 50 irradiation cycles and c) for 30 wt% Au NP on ZnO after every second cycle during first 10 passages; d) ratio of absorption to scattering K/S determined from Kubekla-Munk theory for pure ZnO before and after 50 passages PLML and for 30 wt% Au NP on ZnO before and after 50 passages PLML, respectively

UV-vis spectra in Fig. 3 show the difference between PLML of pure ZnO and for PLML of 30 wt% Au NP with ZnO. Evolution of the local peak around 600 nm can be attributed to scattering of light on formed spheres with sizes in this wavelength regime. This scattering effect occurs for pure ZnO SMS and for ZnO SMS with included Au NP. An increase of UV extinction for pure ZnO is also observed during PLFL due to formation of defect-rich ZnO particles [20]. The ZnO SMS obtained after PLML appear yellowish, similar to defect-rich, bandgap-shifted ZnO particles derived from PLFL of ZnO [20]. Thus we attribute the increased UV extinction to the formation of defect-rich ZnO SMS what is supported by fluorescence measurements shown in Fig. S6. For inclusion of Au NP into ZnO SMS this distinctive increase of UV extinction is not observed. Instead a second extinction peak around 400 nm to 430 nm occurs. Based on the Kubelka-Munk equations [30, 31] we determined the ratio of absorption to scattering K/S from the diffuse reflection spectra, shown in Fig. 3 d). Absorption caused by plasmon resonance of Au NP around 540 nm can be observed for educt particles as well as for Au NP inclusions in ZnO SMS. The plasmon peak of the Au/ZnO educt is boarder and less distinctive due to smaller Au NP on ZnOs surface (see Fig. S7 and S8, 0 passages). After 50 passages of PLML this Au NP is more distinctive due to size increase of gold. From the diagram in Fig. 3 d) we determined the bandgap of the different educts and products. Diagrams and linear fits for determination of band gap energy, based on Kubelka-Munk equation and absolute values of diffuse reflection spectra are shown in Fig. S9 in supporting information. Determination of bandgap energy shows that for both pure ZnO before and after 50 passages of PLML as well as for untreated 30 wt% Au NP on ZnO the bandgap energy is around 3.23 eV (~384 nm). When Au NP are included into ZnOs matrix this value decreases to around 3.07 eV (~404 nm). This is in agreement witch Chanu et al. who integrated Au clusters into ZnO [32]. In similar, the preservation of plasmon resonance for integrated plasmonic silver nanoparticles into TiO_2 and related photocatalytic activity was demonstrated by Awazu et al. [33]. The Au NP integrated into ZnO SMS also possess plasmonic properties shown in Fig. 3 d).

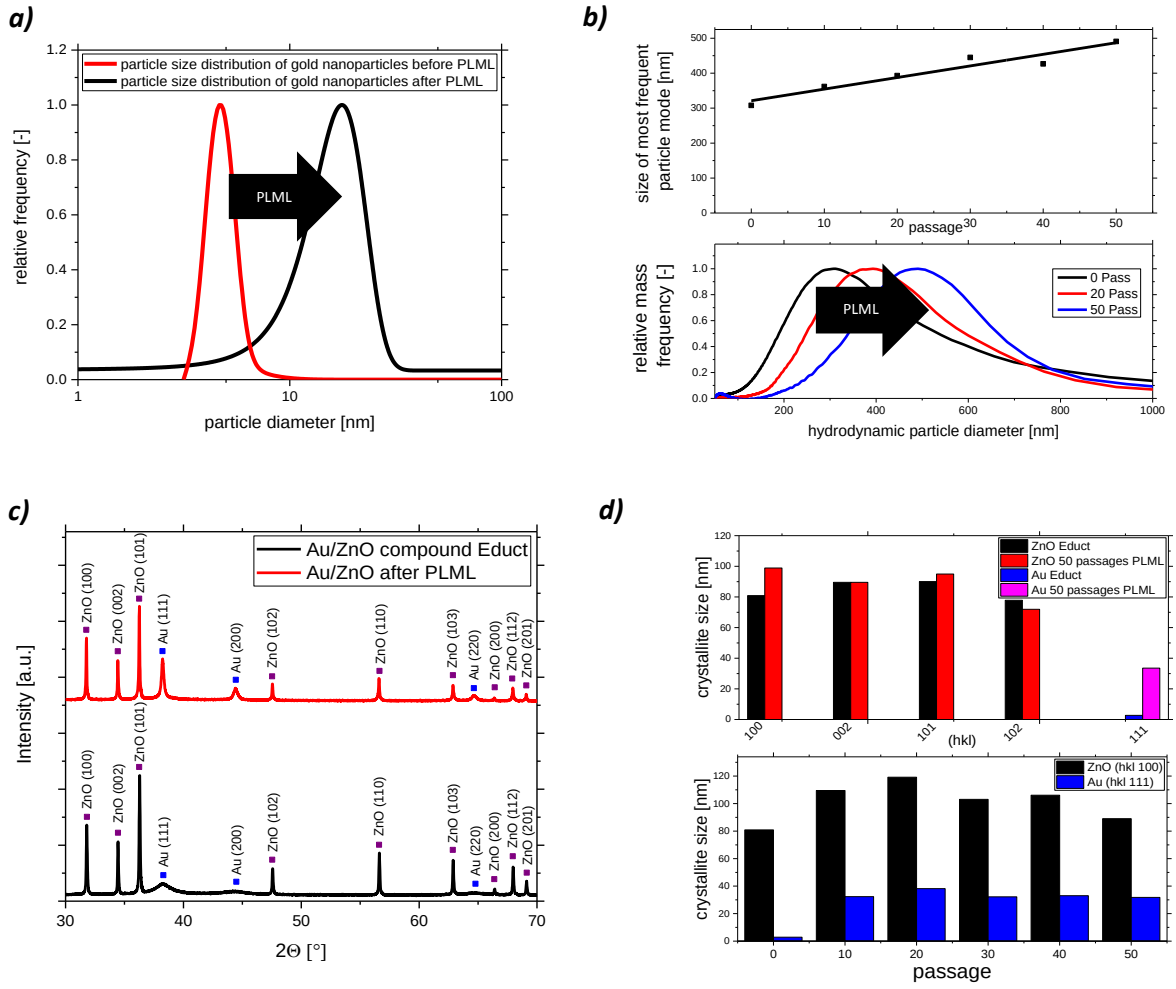

Fig. 4 a) particle size distribution of gold nanoparticles before (red curve, supported on zinc oxide) and after (black curve, integrated into zinc oxide sub-micrometer spheres) PLML detected by analytical disc centrifuge measurements (before PLML) and determined by a Gaussian fit from histograms taken from SEM images (after PLML) for 30 wt%; b) size shift and particle size distribution of the 30 wt% Au NP on ZnO compound after 0, 20 and 50 passages; c) XRD pattern of the gold zinc oxide compound with 30 wt% Au NP before and after 50 passages exposed to PLML conditions and d) cristallite size calculated from the XRD pattern and evolution of crystallite size after each 10 passages from 0 to 50 irradiation cycles

Obviously, during PLML of supported Au NP on ZnO a significant increase of Au NP size is observed at almost constant ZnO volume. Fig. 4 a) shows the particle size distribution of gold nanoparticles before and after PLML. The size of Au NP measured by SEM (see Fig. S4) increases after PLML from ~5 nm to ~17 nm, by about a factor of 3. This means that zinc oxide microparticles and gold nanoparticles obviously have been transferred into a molten state and both resolidify as spheres with gold granules inside ZnO. The evolution of crystallite size shown in Fig. 4 d) proves that already after 10 passages Au NP with diameters around 30-40 nm are formed and do not chance significantly during the additional passages. Increase of Au NP size causes shift of surface plasmon resonance wavelength and increase of intensity. Thus embedding plasmonic particles into semiconductors causes enhancement of light absorption, becoming naturally more distinct if size of Au NP is increased, as known for silver nanoparticles integrated into semiconductors [34]. XRD pattern reveal crystallinity of the two materials whereby a size increase of the gold nanoparticles is confirmed (Fig. 4 c) and d)). SEM images in Fig. 5 c) and d) validate fabrication of sub-micrometer spheres for zinc oxide with 5 wt% Au NP and 30 wt% Au NP at a laser fluence of ~ 80 mJ/cm² at liquid jets' surface. This is in agreement to Tsuji et al. who observed similar SMS particle sizes after PLML at 100 mJ/cm² [12]. At laser fluences of 380 mJ/cm² or higher no PLML can be observed (see Fig. 2 a) and Fig. S3) tested for pure ZnO. But a reduction in hydrodynamic particle diameter occurs (starting at laser fluences above ~ 200 mJ/cm²), confirmed by ADC analysis of hydrodynamic particle diameter shown in Fig. S5. For lower laser fluences no or only slight increase in particle size is obtained, indicating an almost isochoric particle melting (of primary particles and aggregates) and resolidification, similar to the findings on particle reshaping by Nakamura et al. and Liu et al. [13, 23].

Integration of the Au NP into the volume of its ZnO support was determined by correlated SEM images taken both with a secondary electron detector and a back scattered electron detector (Fig. 5 c), d)).

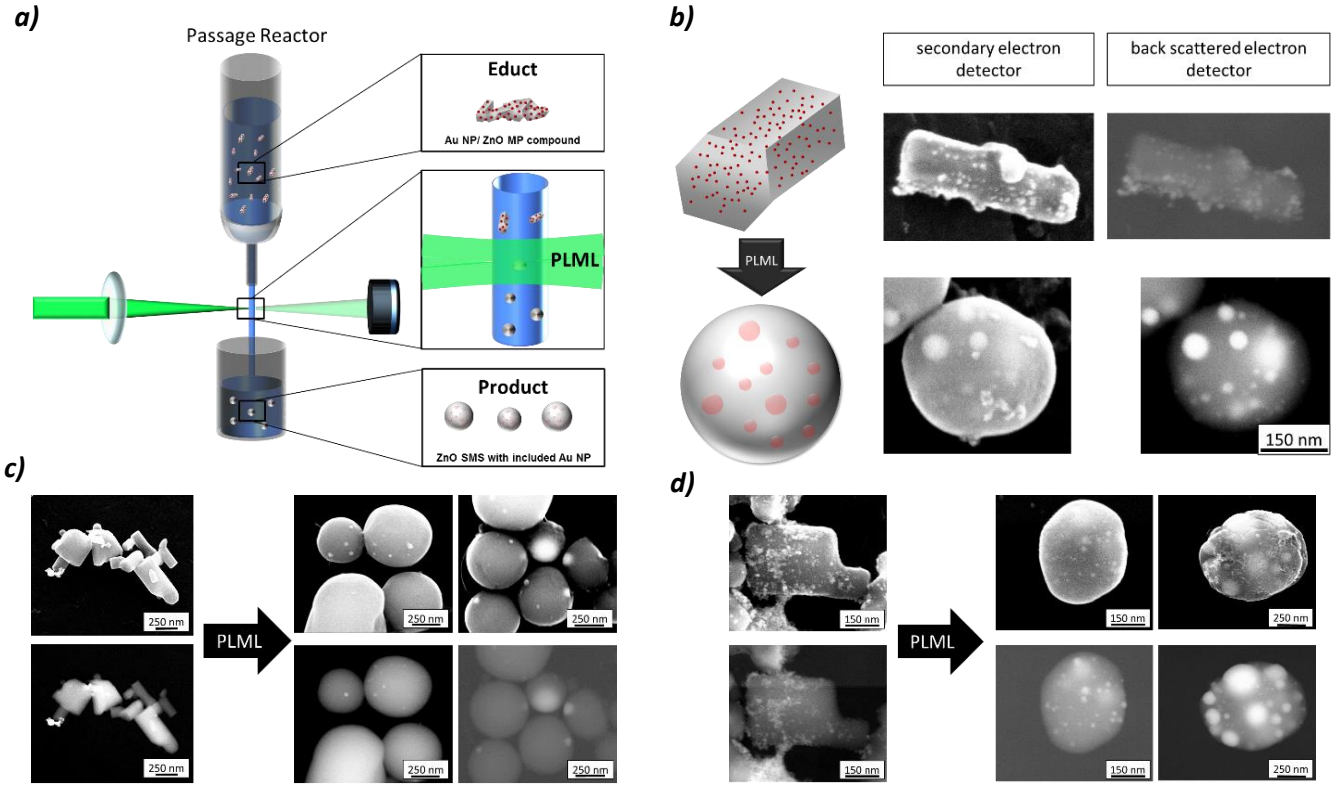

Fig. 5 a) illustration of the set-up for laser irradiation of particles in a free liquid flow changing particles morphology from educt to product during PLML; b) schematic illustration of the Au NP/ZnO MP compound before PLML with nanoparticles onto the support and after PLML with inclusion of nanoparticles (left) and SEM images of corresponding particles (right); c) zinc oxide particles with 5 wt% of gold nanoparticles before (left) and after (right) PLML (50 passages) imaged with a secondary electron detector (top row) and a back scattered electron detector (bottom row); d) zinc oxide particles with 30 wt% of gold nanoparticles before (left) and after (right) PLML (50 passages) imaged with a secondary electron detector (top row) and a back scattered electron detector (bottom row)

The former is more sensitive to surface topography (lower penetration depth of electrons) and the latter is more sensitive to elemental contrast (higher penetration depth), thus depicting Au NP in higher contrast to zinc oxide.

Additional SEM images are shown in Fig. S7 and S8. A quantitative transformation of surface-adsorbed gold into inclusions inside zinc oxide sub-micrometer spheres is obtained after 50 passages of laser irradiation with 80 mJ/cm². SEM images showing the evolution of Au NP inclusion into ZnO SMS after each 10 passages are depicted in Fig. S10.

Regarding the control of the educt mass flow, Figure 5 a) illustrates the process of PLML in a sequential liquid flow with defined volume flow rates. The liquid jet is formed by a capillary and the laser is focused perpendicular on the liquid. Particles passing the irradiated volume are transferred into the molten state. Fig. 5 d) shows that different sizes of included Au NP can be obtained. Due to cumulation of irradiation cycles (passages) it might be possible that previously formed SMS are remolten thus giving the possibility of Au NP fusing to larger NP. Figure 5 b) sketches the transformation from supported Au NP onto ZnO towards Au NP inclusions within ZnO SMS by PLML, with corresponding SEM images. SEM images before PLML and after 10, 30 and 50 passages, shown in Fig. 6 a), demonstrate that Au NP size increases already after 10 passages and are not completely included into the ZnO matrix in the intermediate state of the processing. This formation of crystalline Au NP is in agreement with sizes determined by XRD peak analysis, shown in Fig. 4 d). Scherrer equation reveals that crystalline Au NP with diameters around 30 nm from already after 10 passages and do not change their size significantly afterwards. The SEM images after 10 passages (Fig. 6 a)) demonstrate different appearance of non-included and included Au NP. After 30 and 50 passages no more Au NP absorbed on ZnO particles surface are absorbed, but their inclusion into the ZnO spheres is obvious. A mechanistic hypothesis of process evolution is illustrated in Fig. 6 b).

From UV-vis spectra it can be concluded that generated Au/ZnO hybrid SMS feature interesting optical properties with two local extinction peaks as known for gold nanorods but with completely spherical particles.

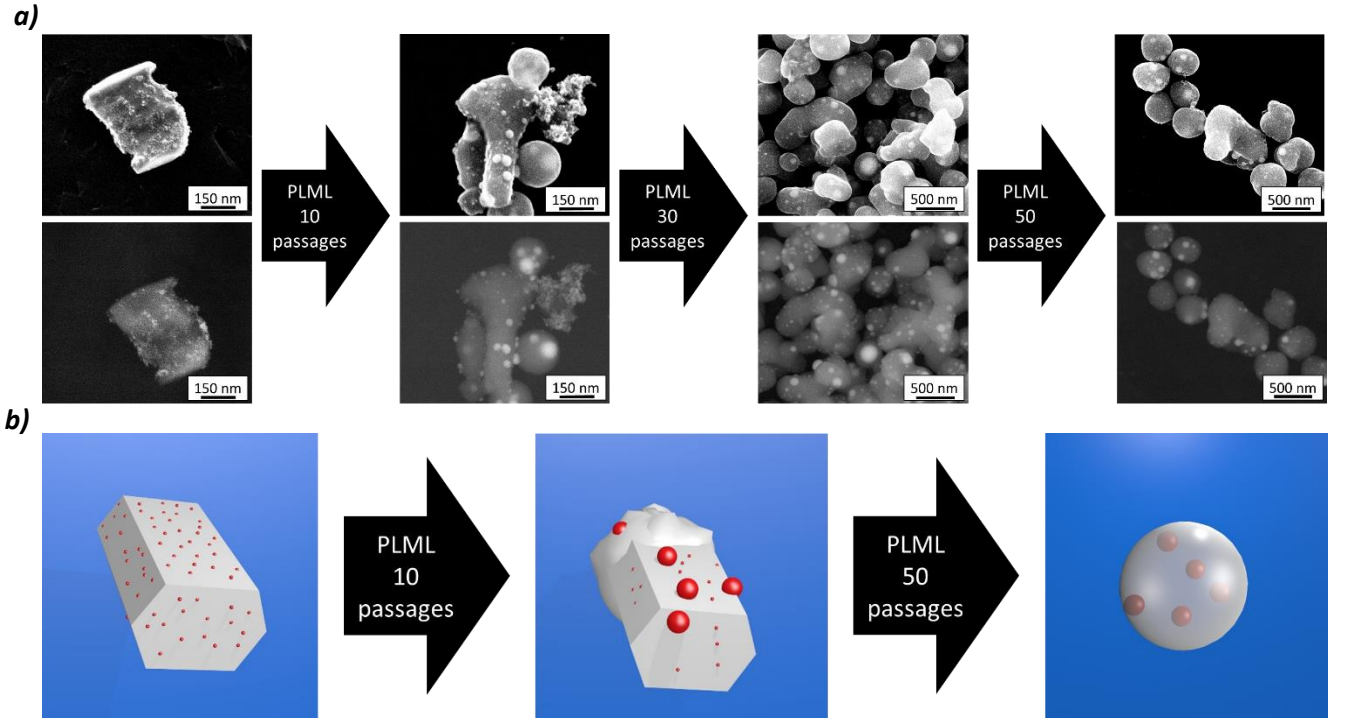

Fig. 6 Evolution of crystalline Au NP inclusion into their ZnO support for different number of irradiation passages; a) SEM images of educt (left) and after 10, 30 and 50 passages of PLML detected witch a secondary electron detector (top images) and a back scattered electron detector (bottom images) showing evolution of Au (bright) and ZnO particle morphology b) schematic illustration of the evolution from the adsorbed Au NP on ZnO (educt) via intermediate state with size-increased Au NP (see XRD in Fig. 4) on reshaped ZnO towards included Au NP into the spherical ZnO matrix (product)

Conclusions

In summary, integration of metals, in particular plasmonic nanoparticles into a submicron-confined semiconductor (or dielectric) volume is challenging but could provide unique structural and optical properties. Here it is shown that pulsed laser melting of supported gold/zinc oxide particles enables embedding of plasmonic nanoparticles into a semiconductor matrix isochorically forming monomodal sub-micrometer spheres. The use of monodisperse and ligand-free gold nanoparticles allowed to attach high nanoparticle loads onto zinc oxides surface and to investigate its structural inversion. During processing gold nanoparticles first increase in size and are subsequently transferred during additional irradiation passages into their spherical support. The investigation of structural morphology and the elemental contrast of the particles by correlated electron microscopy confirmed the integration of the metal nanoparticle into the semiconductor solid spheres. The liquid flow passage reactor allows to characterize the material properties after each passage with a defined laser energy dose [20], providing sequential "snapshots" on the evolution of the process and mechanistic insight into pulsed laser melting of supported particles. Hence nanoparticulate surface adsorbates, widely available as raw materials for catalysis, have been integrated as solid inclusion into their support.

Acknowledgements

We thank Bernardo Oliviera de Viestel for experimental support during PLML of the gold/zinc oxide hybrid particles.

References

1 M. Stratakis and H. Garcia, *Chem. Rev.*, 2012, **112**, 4469-4506
2 W. Yu, M. D. Porosoff and J. G. Chen, *Chem. Rev.*, 2012, **112**, 5780-5817
3 J. C. Meier, C. Galeano, I. Katsounaros, J. Witte, H. J. Bongard, A. A. Topalov, C. Baldizzone, S. Mezavilla, F. Schüth and K. J. J. Mayrhofer, *Beilstein J. Nanotechnol.*, 2014, **5**, 44-67
4 J. Strunk, K. Kaehler, X. Xia, M. Comotti, F. Schueth, T. Reinecke and M. Muhler, *Appl. Catal. A*, 2009, **359**, 121-128
5 P. Li, Z. Wei, T. Wu, Q. Peng and Y. Li, *J. Am. Chem. Soc.*, 2011, **133**, 5660-5663
6 M. Lau, R. G. Niemann, M. Bartsch, W. O'Neill and S. Barcikowski, *Appl. Phys. A*, 2014, **114**, 1023-1030
7 Y. Ishikawa, Y. Shimizu, T. Sasaki and N. Koshizaki, *Appl. Phys. Lett.*, 2007, 91, 161110 3pp
8 H. Wang, N. Koshizaki, L. Li, L. Jia, K. Kawaguchi, X. Li, A. Pyatenko, Z. Swiatkowska-Warkocka, Y. Bando and D. Goldberg, *Adv. Mater.*, **2011**, 23, 1865-1870
9 X. Hu, H. Gong, Y. Wang, Q. Chen, J. Zhang, S. Zheng, S. Yang and B. Cao, *J. Mater. Chem.*, 2012, **22**, 15947-15952
10 H. Fujiwara, R. Niyuki, Y. Ishikawa, N. Koshizaki, T. Tsuji and K. Sasaki, *Appl. Phys. Lett.*, 2013, **102**, 061110 4pp

11 H. Wang, K. Kawaguchi, A. Pyatenko, X. Ki, Z. Swiatkowska-Warkocka, Y. Katou and N. Koshizaki, *Chem. Eur. J.*, 2012, **18**, 163-169
12 T. Tsuji, Y. Higashi, M. Tsuji, H. Fujiwara, Y. Ishikawa and N Koshizaki, *J. Laser Micro. Nanoen.*, 2013, **8**, 292-295
13 D. Liu, C. Li, F. Zhou, H. Zhang, X. Li, G. Duan, W. Cai and Y. Li, *Sci. Rep.*, 2014, **5**, 7686 9pp
14 S. Link and M. A. El-Sayed, *J. Phys. Chem. B*, 1999, **103**, 8410-8426
15 S. Link and M. A. El-Sayed, *J. Phys. Chem. B*, 1999, **103**, 4212-4217
16 S. Link, C. Burda, M. B. Mohamed, B. Nikoobakht and M. A. El-Sayed, *J. Phys. Chem. A*, 1999, **103**, 1165-1170
17 S. Inasawa, M. Sugiyama and Y. Yamaguchi, *J. Phys. Chem. B*, 2005, **109**, 3104-3111
18 T. Tsuji, T. Yahata, M. Yasutomo, K. Igawa, M. Tsuji, Y. Ishikawa and N. Koshizaki, *Phys. Chem. Chem. Phys.*, 2013, **15**, 3099-3107
19 T. Tsuji, Y. Higashi, M. Tsuji, Y. Ishikawa and N. Koshizaki, *Appl. Surf. Sci.*, 2015, **348**, 10-15
20 M. Lau and S. Barcikowski, *Appl. Surf. Sci.*, 2015, **348**, 22-29
21 Y. Ishikawa, Q. Feng and N. Koshizaki, *Appl. Phys. A*, 2010, **99**, 797-803
22 Z. Swiatkowska-Warkocka, K. Koga, K. Kawaguchi, H. Wang, A. Pyatenko and N. Koshizaki, *RSC Adv.*, 2013, **3**, 79-83
23 M. Nakamura, A. Oyane, I. Sakamaki, Y. Ishikawa, Y. Shimizu and K. Kawaguchi, *Phys. Chem. Chem. Phys.*, 2015, **17**, 8836-8842
24 K. Kawaguchi, J. Jaworski, Y. Ishikawa, T. Sasaki and N. Koshizaki, *IEEE Trans. Magn.*, 2006, **42**, 3620-3622
25 K. Kawaguchi, J. Jaworski, Y. Ishikawa, T. Sasaki and N. Koshizaki, *J. Magn. Magn. Mater.*, 2007, **310**, 2369-2371
26 Z. Swiatkowska-Warkocka, K. Kawaguchi, Y. Shimizu, A. Pyatenko, H. Wang and N. Koshizaki, *Langmuir*, 2012, **28**, 4903-4907
27 P. Wagener, A. Schwenke and S. Barcikowski, *Langmuir*, 2012, **28**, 6132-6140
28 G. Marzun, J. Nakamura, X. Zhang, S. Barcikowski and P. Wagener, *Appl. Surf. Sci.*, 2015, **348**, 75-84
29 P. Stamatakis, B. R. Palmer, G. C. Salzmanm C. F. Bohren and T. B. Allen, J. Coat. Technol., 1990, **62**, 95-98
30 P. Kubelka and F. Munk, Z. Tech. Phys., 1931, **12**, 593-601
31 P. Kubelka, *J. Opt. Soc. Am.*, 1948, **38**, 448-457
32 T. I. Chanu, T. Muthukumar and P. T. Manoharan, *Phys. Chem. Chem. Phys.*, 2014, **16**, 23686--23698
33 K. Awazu, M. Fujimaki, C. Rockstuhl, J. Tominaga, H. Murakami, Y. Ohki, N. Yoshida and T. Watanabe, *J. Am. Chem. Soc.*, 2008, **130**, 1676-1680
34 P. Spinelli and A. Polman, *Opt. Express*, 2012, **20**, A641-A654